Inorganic Chemistry

Article

pubs.acs.org/IC

Quantitative Vibrational Dynamics of the Metal Site in a Tin Porphyrin: An IR, NRVS, and DFT Study

Bogdan M. Leu,*[,†] Marek Z. Zgierski,[‡] Christian Bischoff,[§] Ming Li,[⊥] Michael Y. Hu,[†] Jiyong Zhao,[†] Steve W. Martin,[§] Esen Ercan Alp,[†] and W. Robert Scheidt[⊥]

[†]Advanced Photon Source, Argonne National Laboratory, Argonne, Illinois 60439, United States

[‡]National Research Council of Canada, Ottawa, Ontario K1A OR6, Canada

[§]Department of Materials Science and Engineering, Iowa State University, Ames, Iowa 50011, United States

[⊥]Department of Chemistry and Biochemistry, University of Notre Dame, Notre Dame, Indiana 46556, United States

Supporting Information

ABSTRACT: We used a newer, synchrotron-based, spectroscopic technique (nuclear resonance vibrational spectroscopy, NRVS) in combination with a more traditional one (infrared absorption, IR) to obtain a complete, quantitative picture of the metal center vibrational dynamics in a six-coordinated tin porphyrin. From the NRVS ^{119}Sn site-selectivity and the sensitivity of the IR signal to ^{112}Sn/^{119}Sn isotope substitution, we identified the frequency of the antisymmetric stretching of the axial bonds (290 cm^{-1}) and all the other vibrations involving Sn. Experimentally authenticated density functional theory (DFT) calculations aid the data interpretation by providing detailed normal mode descriptions for each observed vibration. These results may represent a starting point toward the characterization of the local vibrational dynamics of the metallic site in tin porphyrins and compounds with related structures. The quantitative complementariness between IR, NRVS, and DFT is emphasized.

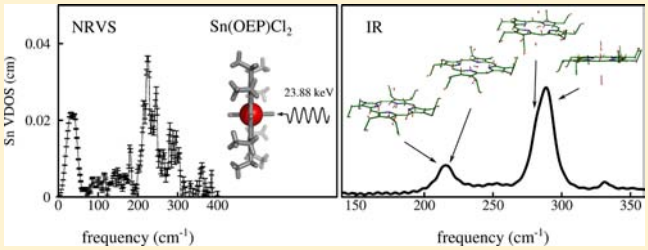

INTRODUCTION

Tin porphyrins, historically important compounds for revealing the extent to which the porphyrin ring can expand,[1,2] have been showcased among other M(IV) porphyrins for their particular combination of chemical and spectroscopic properties,[3] as well as for their numerous practical applications. In medicine, for example, they are used in the treatment of various diseases and conditions associated with increased heme oxygenase activity[4] and as inhibitors of HIV-1 infections.[5] In inorganic chemistry, they serve as components for molecular motors,[6,7] molecular timepieces,[8] and as building blocks for complex supramolecular architectures.[9] Despite having such diverse applications, vibrational spectroscopy studies of tin porphyrins are scarce, especially for low frequencies.[10,11] To the best of our knowledge, only one vibration below 500 cm^{-1} was previously assigned[11] (tentatively as porphyrin deformation and Sn−N stretching in the Raman spectra of Sn tetraphenyl compounds). In this study, we concentrate primarily on the low-frequency window to obtain a complete, quantitative picture of the central Sn atom vibrational dynamics in octaethylporphinatodichlorotin(IV) Sn(OEP)Cl$_2$ (Figure 1) from a combination of experimental and computational methods.

On the experimental side, infrared (IR) studies of porphyrins have been carried out for over seven decades.[12] Their rich spectra are fairly well understood (particularly above 400 cm^{-1}), with band assignments having been reported for numerous metalloporphyrins with various metal centers, peripheral groups, and axial ligands, as well as for metal-free compounds. Much newer[13−15] is the synchrotron-based nuclear resonance vibrational spectroscopy (NRVS) technique,[16,17] also known as nuclear inelastic scattering (NIS) or nuclear resonant inelastic X-ray scattering (NRIXS), available only at a few third-generation synchrotron facilities. NRVS takes advantage of tunable, highly brilliant, stable X-ray beams to target a specific (Mössbauer) isotope, regardless of the complexity of the molecule investigated. It yields quantitative information about the dynamics of the atom of interest and the elasticity of its environment. NRVS identifies *all* the vibrations associated with the respective site and represents a valuable complementary tool to more traditional techniques, such as IR and Raman

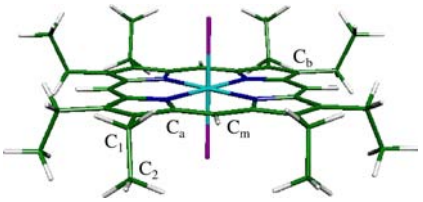

Figure 1. Predicted structure of Sn(OEP)Cl$_2$. Color scheme: cyan = Sn, blue = N, green = C, magenta = Cl, white = H. This figure and Figure 6 were generated with Molekel,[56] version 4.3.win32.

Received: May 8, 2013
Published: August 20, 2013

   dx.doi.org/10.1021/ic401152b | *Inorg. Chem.* 2013, 52, 9948−9953

spectroscopies. Unlike these techniques, NRVS is not hampered by selection rules or solvent interference, and it is virtually background-free. The most studied isotope is ^{57}Fe, because of the importance of iron in biology (e.g., as the center of the active site in heme proteins), inorganic chemistry (as the central atom in porphyrins used as mimics of the respective active sites), geophysics (iron is the main component of the Earth's interior), and condensed matter physics. However, a handful of other isotopes can be measured,[16] including ^{119}Sn.[18,19] On the computational side, density functional theory (DFT) calculations predict the atomic structure with great accuracy (see Table S3 in the Supporting Information) and describe quantitatively the molecular dynamics by providing the vibrational amplitudes for all atoms. A strong synergy has developed over the past few years between NRVS and DFT. On the one hand, experiments provide a stringent test for the calculations; on the other, the interpretation of the measured spectra benefits from the unique insight provided by the calculations. This complementariness is further emphasized in this study.

METHODS

The NRVS measurements were carried out at beamline 3-ID at the Advanced Photon Source, Argonne National Laboratory. The main components of the setup are typical of a NRVS experiment: a primary monochromator tunes the energy of the incident photons around 23.88 keV (corresponding to a nuclear resonance of the ^{119}Sn isotope); a nested high-resolution monochromator consisting of a pair of Si[4 4 4] and Si[12 12 12] crystals[20] reduces the bandpass to approximately 1 meV; and an avalanche photodiode detects the delayed NRVS signal. The prompt, electronically scattered signal is ignored. The sample was loaded in a cryostat. The temperature, determined from the detailed balance condition, was 160 K. We collected 10 scans in the −30−70 meV range (≈−240−560 cm^{-1}) with a 0.25 meV step. Data analysis consists of the normalization of the measured signal according to Lipkin's sum rules[21] and of the extraction of the partial vibrational density of states (VDOS) $D(\bar{\nu})$.[22]

We ran the IR measurements (Bruker IFS 66 v/s) under vacuum on samples diluted to ∼8% in CsI pressed pellets. We used a KBr beamsplitter and germanium-coated Mylar beamsplitter for the mid-IR (4000−400 cm^{-1}) and far-IR (600−130 cm^{-1}) ranges, respectively. We gathered 128 scans at 2 cm^{-1} resolution.

DFT calculations were performed with Gaussian98,[23] using B3LYP functionals of the DFT theory and with the DZVP (DFT orbital) basis sets for every atom.

RESULTS AND DISCUSSION

Figure 2 shows the IR spectra of ^{112}Sn(OEP)Cl$_2$ and ^{119}Sn(OEP)Cl$_2$. The bands above 3000 cm^{-1} and in the 2900−3000 cm^{-1} region correspond to in-plane C$_m$-H stretching[24] and to C−H vibrations within the ethyl groups,[25] respectively. The bands in the 600−1500 cm^{-1} frequency range, on the other hand, are due to motions of the ethyl groups (scissoring, wagging, twisting, and rocking) and of the porphyrin ring (in-plane and out-of-plane).[26] We list the frequencies of the main bands of the ^{119}Sn compound in Table S1 in the Supporting Information, together with their assignments based on comparisons with related molecules, such as Ge(OEP)Cl$_2$, M(OEP), and metal-free OEP.[27]

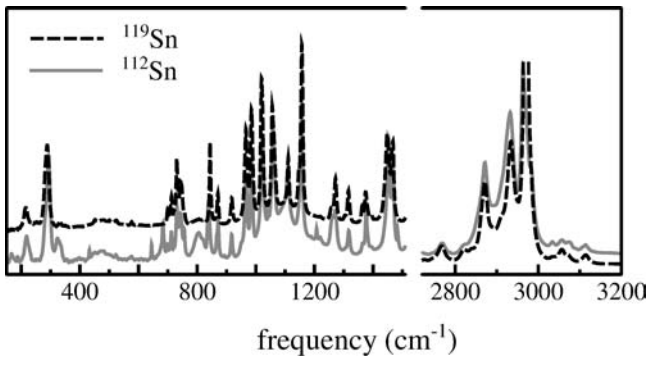

Figure 2. IR spectra of ^{112}Sn(OEP)Cl$_2$ and ^{119}Sn(OEP)Cl$_2$.

Visual inspection of Figure 2 reveals that the two spectra are essentially identical above 400 cm^{-1}, which is indicative of almost nonexistent motions of the Sn atom in the respective modes. In fact, the majority of the main bands are within a few wavenumbers of those reported for a molecule of a similar structure but with a different central metal, Ge(OEP)Cl$_2$.[27] Minor discrepancies between the ^{112}Sn and ^{119}Sn spectra include the presence in the former of weak features around 330 cm^{-1}, between 600 and 700 cm^{-1}, and around 810 cm^{-1} (not present in M(OEP) complexes,[27,28] however, a porphyrin ring mode and an ethyl mode have been reported in this region for Ge(OEP)Cl$_2$). These differences may be due to impurities, slight distortions of the ethyl groups, and/or traces of four-coordinated Sn(OEP). The latter possibility is supported by the 2870 cm^{-1} band, which is present in the spectra of metal-free OEP but disappears in the spectrum of the six-coordinated Ge(OEP)Cl$_2$.

Band assignment is usually carried out via isotope substitution, comparison between the spectra of molecules with similar structures, and computational methods. For the low frequencies, NRVS represents a powerful additional tool to this approach due to its ability to target a specific isotope (^{119}Sn in this case). In this study, we concentrate on the low-frequency region (below 300 cm^{-1}), which is expected to correspond to vibrations of the metal−ligand bonds.[29,30]

The complete Sn VDOS spectrum yielded by NRVS is shown in Figure 3. The quantitative nature of NRVS is underscored by the fact that the area of each peak is equal to a quantity named mode composition factor $e^2_{j\alpha}$,[17,31] defined as the fraction of the total kinetic energy of mode α associated with motion of atom j. The individual peaks and the corresponding e^2_{Sn} values are listed in Table 1.

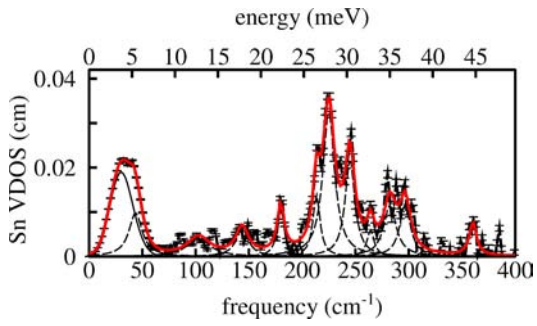

Figure 3. Sn VDOS from the NRVS experiment. Black continuous line indicates fitted log-normal attributed to lattice modes. The other individual peaks (Lorentzians) are shown as black dashed lines and the total fit as a red continuous line.

Although common IR and NRVS modes have been previously observed,[32,33] the mode composition factor represents a valuable additional, quantitative link between NRVS and more traditional vibrational methods (IR, Raman).

dx.doi.org/10.1021/ic401152b | Inorg. Chem. 2013, 52, 9948−9953

Table 1. Frequencies (in cm^{-1}) of the Measured IR and NRVS Bands, and of the Predicted Modes with Sn Motion; the Mode Composition Factors from the Experiment (IR, eq 1; and NRVS) and the Calculation (eq 2); and the Mode Description (ip.=in-plane)

IR, $^{119/112}$Sn	e^2_{Sn}	NRVS	e^2_{Sn}	DFT	e^2_{Sn}	description
		30	0.51			lattice modes
		44	0.22	29	0.22	γ_9
		103	0.16			
		144	0.14	121	0.21	γ_8
		180	0.13	149, 153	0.16	Sn ip., C_b-C_1 rock.
215.8/218.8	0.47	213	0.17	218, 219	0.47	γ_7 (219 only), Sn, CH_3
		225	0.67	209	0.28	Sn ip., CH_3
				231	0.04	CH_3
		245	0.37	253, 256	0.36	Sn ip., pyr. tilt, ethyl
		264	0.07	273	0.17	Sn ip., pyr. tilt
282.9/283.3	0.05	282	0.25	284	0.17	Sn ip., γ(C_a-C_m), ethyl
290.1/293.5	0.40	297	0.22	301	0.27	ν(Cl–Sn–Cl)$_{asym}$
		360	0.09	347, 358	0.06	C_b-C_1 sciss. +pyr. tilt/ γ(C_a-C_m)

For a mode α, it can be estimated from the frequency shift $\Delta\bar{\nu}_\alpha$ due to a change Δm_j in the mass of atom j[31]

$$e^2_{j\alpha} = -2\frac{d(\ln \bar{\nu}_\alpha)}{d(\ln m_j)} \approx -2\frac{\Delta\bar{\nu}_\alpha/\bar{\nu}_\alpha}{\Delta m_j/m_j} \quad (1)$$

Both features in the IR spectra below 400 cm^{-1} (consisting of a total of three bands) are isotope-sensitive (Figure 4a, b, Table 1) and are due to vibrations of the metal–ligand bonds. Using eq 1, one can extract the overall contribution of the IR-active modes to the NRVS VDOS (see also the Supporting Information), similar to the contributions due to Raman-active modes in previous studies.[34,35] The total e^2_{Sn} value due to the IR-active modes is 0.92 (Table 1), representing ~55% of the Sn VDOS between 190 and 320 cm^{-1} (Figure 4c).

Using the knowledge gained from previous NRVS studies on single-crystal iron porphyrins[36–38] and heme proteins,[39] we attribute the feature that dominates the NRVS signal (≈200–280 cm^{-1}) primarily to in-plane modes, i.e., to vibrations of the central Sn in the plane of the porphyrin core. This initial interpretation will be later confirmed by the calculations. On the other hand, the 290 cm^{-1} band in the ^{119}Sn(OEP)Cl_2 IR spectrum meets the requirements for the antisymmetric Cl–Sn–Cl stretching mode: strong IR intensity and a corresponding strong NRVS signal due to the significant Sn motion involved.

We gain further insight into the Sn dynamics from DFT calculations. DFT predicts the molecular structure and the mean square displacement r of all atoms for each vibrational mode. There is good agreement between measured and predicted structural parameters (see Table S3 in the Supporting Information), with bond lengths being overestimated by less than 2%. DFT yields the mode composition factor $e^2_{j\alpha}$ for each atom according to[40]

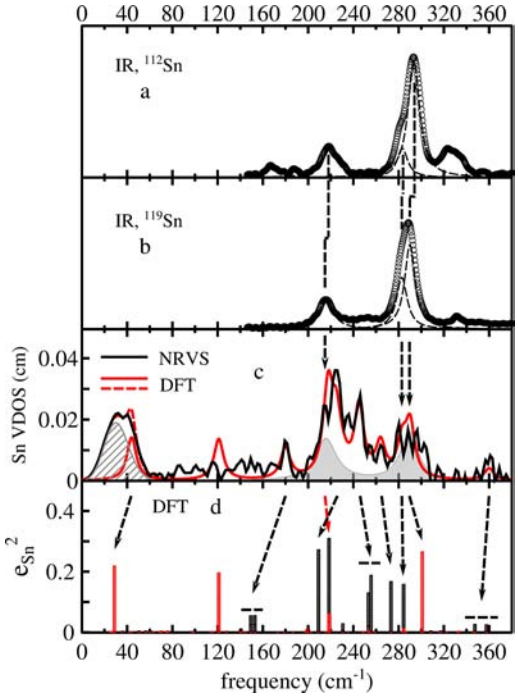

Figure 4. Experimental and computational results. (a, b) IR spectra of ^{112}Sn(OEP)Cl_2 and ^{119}Sn(OEP)Cl_2, respectively (open squares), including the individual peaks (dashed lines). (c) Sn VDOS from NRVS (black line) and DFT (eq 3, red continuous line) based on the correspondence indicated with arrows (a similar comparison without manually adjusting the predicted frequencies is shown in Figure S1a in the Supporting Information). The dashed red line includes the contribution from the lattice modes as well (cross-hatched). The solid gray area represents the contribution to the NRVS signal from the IR-active modes. d: Predicted Sn mode composition factors (eq 2, Table 1, and Table S4 in the Supporting Information). Black (red) bars: in-plane (out-of-plane) modes.

$$e^2_{j\alpha} = \frac{m_j r_j^2}{\sum m_i r_i^2} \quad (2)$$

where the sum is over all the atoms. Therefore, e^2_{Sn} represents the common denominator of the two experimental and one computational techniques used in this study. Table S4 in the Supporting Information lists all the predicted modes involving Sn motion, their IR intensity, the e^2_{Sn} value for each axis direction (obtained by replacing r with x, y, and z in the numerator of eq 2[35,41]), and the total e^2_j for other atoms or groups of atoms (also shown in Figure 5). The x and y directions are in the plane of the porphyrin core, whereas z is perpendicular to it. The $\sum e^2_j$ (j = Sn, Cl, N, C, ethyl) values provide a quantitative way of describing the predicted modes, in addition to mode visualization (Figure 6).

Sn in-plane and out-of-plane motions are shown in Figure 4d as black and red bars, respectively. No Sn modes are predicted above 360 cm^{-1}, validating the energy range chosen for the NRVS measurements and confirming the insensitivity of the IR spectra above 400 cm^{-1} to the nature of the Sn isotope (Figure 2). It is worth mentioning that the ethyl groups have large contributions to most of the Sn modes, accounting for as much as 84% of their kinetic energy (see Table S4 in the Supporting Information).

For atom j, the VDOS is predicted according to

dx.doi.org/10.1021/ic401152b | Inorg. Chem. 2013, 52, 9948–9953

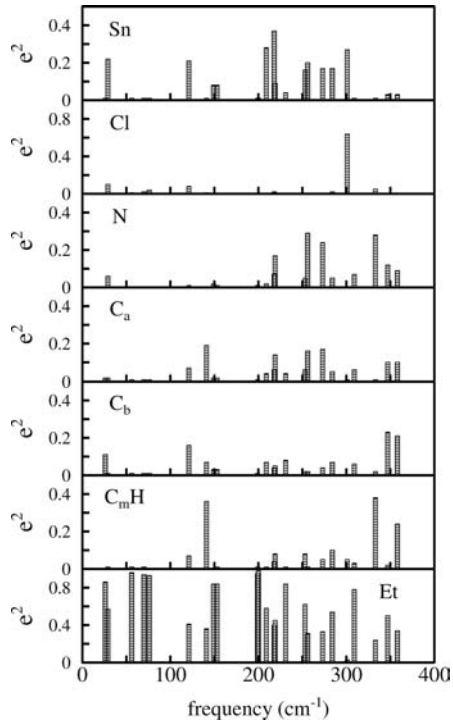

Figure 5. Predicted kinetic energy distribution over Sn, Cl, C, N, and ethyl (Et) atoms (CH_2–CH_3). See also Table S4 in the Supporting Information.

$$D(\bar{\nu}) = \sum e_{j\alpha}^2 \mathcal{L}(\bar{\nu} - \bar{\nu}_\alpha) \quad (3)$$

where $\mathcal{L}(\bar{\nu} - \bar{\nu}_\alpha)$ is a normalized line shape function. For Sn, $D(\bar{\nu})$ can be compared directly with the experimental VDOS on an absolute scale. To facilitate this comparison, in eq 3 a Lorentzian line shape with full width at half-maximum Γ=10 cm^{-1} for $\mathcal{L}(\bar{\nu} - \bar{\nu}_\alpha)$ was used.

Above 200 cm^{-1}, the discrepancies between the calculated and the observed NRVS frequencies are on the order of a few percent (Table 1), which is typical for such predictions on similar molecules containing ^{57}Fe (larger differences have been reported for Fe-axial ligands modes, such as Fe-NO stretch[40,42]). The effect of the nature and the orientation of the peripheral groups on the NRVS spectrum and, consequently, the importance of including them in the calculations has been demonstrated previously.[40,42,43] With this result in mind, we carried out calculations on various Sn(OEP)Cl_2 conformers and found that the orientation of the ethyl groups with respect to the porphyrin plane considerably influences the accuracy of the predictions: only the correct structure[44,45] reproduces the overall pattern of the measured spectrum (see Figure S1 in the Supporting Information).

A comparison between the measured and the calculated Sn VDOS is shown in Figure S1a in the Supporting Information. By manually adjusting the frequencies of the predicted modes (the correspondence is indicated with arrows in Figure 4d), an excellent qualitative and quantitative agreement between experiment and theory is obtained up to 80 cm^{-1} and above 150 cm^{-1} (Figure 4c), as is further discussed below.

The predicted frequency of the ν(Cl–Sn–Cl)$_{asym}$ mode is 301 cm^{-1} (Figure 6). Consistent with the experimental results, it has the largest IR intensity in this frequency range and involves large Sn and Cl motions (see Table S4 in the Supporting Information, Figure 5). In fact, most of the kinetic

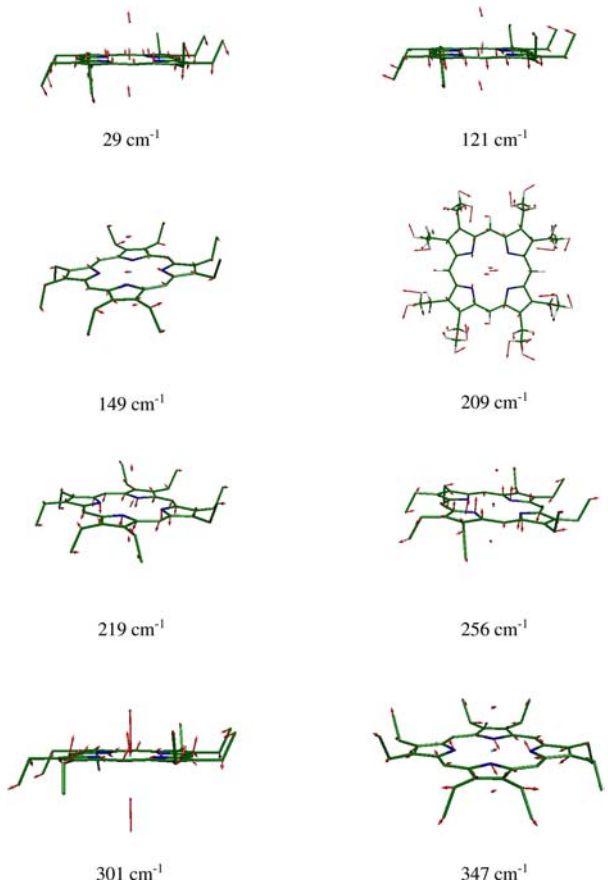

Figure 6. Select predicted modes with Sn motion. Color scheme is the same as in Figure 1. With the exception of the 209 cm^{-1} mode, which involves significant CH_3 motion, hydrogen atoms are omitted for clarity.

energy of this mode (91%) is localized on this particular vibration. A nearby mode (284 cm^{-1}) has a smaller IR intensity (similar to the experiment) and consists of in-plane Sn oscillations, C_mH wagging, and ethyl vibrations. It seems natural to ascribe these two modes to the 290.1 and 282.9 cm^{-1} bands, respectively, in the IR spectrum of the ^{119}Sn-enriched compound. Inspection of Figure 4c reveals an almost perfect agreement between the measured VDOS, the contribution due to IR-active modes, and the predicted VDOS in the 270–320 cm^{-1} region. Quantitatively, the total e_{Sn}^2 values for this cluster obtained from NRVS, IR, and DFT (Table 1) are very close (0.47, 0.45, and 0.44, respectively), underscoring the self-consistency of the three methods employed.

The 215.8 cm^{-1} IR band is sensitive to Sn isotope substitution (it shifts to 218.8 cm^{-1} in the ^{112}Sn spectrum) and therefore contributes to the NRVS signal (Figure 4c). The calculations predict two modes (218 and 219 cm^{-1}) with IR intensity and identical Sn out-of-plane motions ($(e_{Sn}^2)_z$ = 0.06) accompanied by oscillations of the 16 members of the inner ring in the opposite direction, resembling a mode of γ_7 character.[46] However, Sn motion has a much larger in-plane component in the 218 cm^{-1} mode compared to the 219 cm^{-1} mode ($(e_{Sn}^2)_x$ = 0.31 and 0.03, respectively). Two other modes (209 and 231 cm^{-1}) are predicted in the vicinity. They are dominated by ethyl motions ($\sum_{Et} e_j^2$ = 0.58 and 0.84, respectively), with the former involving significant in-plane Sn motion as well ($(e_{Sn}^2)_y$ = 0.27). Overall, there is very good

dx.doi.org/10.1021/ic401152b | Inorg. Chem. 2013, 52, 9948–9953

agreement between the experiment and the calculations in the 200−235 cm^{-1} region as well (Figure 4c), as illustrated by the closeness between the measured and the predicted $\sum e^2_{Sn}$ values: 0.84 from NRVS and 0.79 from DFT (Table 1).

The 245 cm^{-1} band in the NRVS spectrum (e^2_{Sn} = 0.37) corresponds to the predicted 253 and 256 cm^{-1} modes ($\sum e^2_{Sn}$ = 0.36), consisting of Sn in-plane motions orthogonal to each other, ethyl vibrations, and, mainly in the latter, pyrrole tilt (notice the large $\sum e^2_{N}$ and $\sum e^2_{C_a}$ values, Table S4 in the Supporting Information and Figure 5). Another predicted in-plane mode (273 cm^{-1}) corresponds to the measured 264 cm^{-1} band, although agreement between the measured and the calculated e^2_{Sn} is not as good as in other cases. We associate the weak 360 cm^{-1} feature to the predicted 347 and 358 cm^{-1} modes, which involve some Sn in-plane motion, C_b-C_1 scissoring, and pyrrole tilt (the latter also involves C_mH wagging).

As reported previously, it is more difficult to find correspondence on a one-to-one basis between the predicted modes and the measured VDOS below 200 cm^{-1}.[36,40,43] However, we propose that the predicted 149 and 153 cm^{-1} modes, in which ethyl vibrations dominate (mainly C_b-C_1 rocking), and the 29 cm^{-1} mode, which resembles the γ_9 mode described elsewhere,[46] correspond to the measured 180 and 44 cm^{-1} bands, respectively. We fitted the measured signal between 60 and 150 cm^{-1} with two peaks with a total area of 0.30, but DFT predicts only one mode (121 cm^{-1}), assigned as γ_8. This situation is reminiscent of that encountered previously in iron tetraphenyl porphyrins, in which the frequency of the predicted mode was between the frequencies of two features in the experimental spectrum.[36] Several predicted modes with Sn motion are shown in Figure 6.

Finally, lattice modes also contribute to the low-frequency measured VDOS. The integrated area from zero to ~40 cm^{-1} is $\sum e^2_{Sn} = 3m_{Sn}/M$ = 0.49, expected for the translation of the entire molecule.[31,47] This value is very close to the area of the first fitted peak (Table 1), shown as a continuous black line in Figure 3. If we add this contribution to the predicted VDOS generated with eq 3 we obtain excellent agreement between the experiment and the calculation below 80 cm^{-1} as well (dashed red line in Figure 4c).

CONCLUSIONS

We obtained the complete vibrational dynamics picture of the tin atom in $Sn(OEP)Cl_2$ using a combination of experimental and computational techniques. We identified all the modes that involve Sn motion and estimated the fraction of the total kinetic energy associated with the metal site, as well as with the porphyrin core and the peripheral groups. This work presents one of the very rare cases in which NRVS is not applied to iron and demonstrates the ability of NRVS to analyze Sn-porphyrin complexes and related molecules. The potency of metalloporphyrins in treating various diseases and conditions is affected by alterations in the central metal atom[48] and in the peripheral groups.[49] These results may represent a starting point for comparative studies of Sn compounds with different peripheral groups and axial ligands, such as heme oxygenase inhibitors $Sn(MPIX)Cl_2$ and $Sn(PPIX)Cl_2$ (MPIX = mesoporphyrin IX; PPIX = protoporphyrin IX); verdohemes;[50,51] and porphyrins with four peripheral coordination sites used in the synthesis of molecular motors.[7,52] Furthermore, and more generally, the ability of IR spectroscopy (and similarly, Raman spectroscopy) to predict a significant portion of the NRVS results can be used to generate the partial VDOS for isotopes that otherwise are not suitable for NRVS, thus providing access to various thermodynamic and elastic parameters.[53] For example, we found that ~50% of the Sn VDOS above 160 cm^{-1} is due to IR-active modes, but this percentage can be higher for nonsymmetric molecules, whose Raman spectra may be sensitive to isotope substitutions of the metallic site.[34,35] (We note that our Raman spectra of $Sn(OEP)Cl_2$, which we have not discussed in this work, revealed no dependence on $^{112}Sn/^{119}Sn$ isotope substitution). This isotope-substitution approach circumvents one of the NRVS's main disadvantages (the small number of isotopes that can be targeted) and can become a useful tool for investigations of diverse compounds, such as Mg porphyrin complexes functioning as photoreceptors for photosynthesis, Zr(IV) chiral complexes,[54] and anticancer metallodrugs containing a wide range of metals.[55]

ASSOCIATED CONTENT

Supporting Information

The description of $^{112}Sn(IV)(OEP)Cl_2$ and $^{119}Sn(IV)(OEP)Cl_2$ synthesis; additional IR and DFT results; and data analysis details. This material is available free of charge via the Internet at http://pubs.acs.org/.

AUTHOR INFORMATION

Corresponding Author

*E-mail: leu@aps.anl.gov.

Notes

The authors declare no competing financial interest.

ACKNOWLEDGMENTS

WRS acknowledges generous support from the NIH (GM-38401). Use of the Advanced Photon Source, an Office of Science User Facility operated for the U.S. Department of Energy (DOE) Office of Science by Argonne National Laboratory, was supported by the U.S. DOE under Contract No. DE-AC02-06CH11357.

REFERENCES

(1) Collins, D. M.; Scheidt, W. R.; Hoard, J. L. *J. Am. Chem. Soc.* **1972**, *94*, 6689−6696.
(2) Scheidt, W. R. Systematics of the Stereochemistry of Porphyrins and Metalloporphyrins. In *The Porphyrin Handbook*; Kadish, K. M., Smith, K. M., Guilard, R., Eds.; Academic: New York, **2000**; Vol. 3, Chapter 16, p 49.
(3) Arnold, D. P.; Blok, J. *Coord. Chem. Rev.* **2004**, *248*, 299−319.
(4) Abraham, N. G.; Kappas, A. *Pharmacol. Rev.* **2008**, *60*, 79−127.
(5) Neurath, A. R.; Strick, N.; Lin, K.; Debnath, A. K.; Jiang, S. *Antivir. Chem. Chemother.* **1994**, *5*, 322−330.
(6) Ghiggino, K. P.; Hutchison, J. A.; Langford, S. J.; Latter, M. J.; Lee, M. A. P.; Lowenstern, P. R.; Scholes, C.; Takezaki, M.; Wilman, B. E. *Adv. Funct. Mater.* **2007**, *17*, 805−813.
(7) Guenet, A.; Graf, E.; Kyritsakas, N.; Hosseini, M. W. *Inorg. Chem.* **2010**, *49*, 1872−1883.
(8) Bhosale, S. V.; Chong, C.; Forsyth, C.; Langford, S. J.; Woodward, C. P. *Tetrahedron* **2008**, *64*, 8394−8401.
(9) Kim, H. J.; Bampos, N.; Sanders, J. K. M. *J. Am. Chem. Soc.* **1999**, *121*, 8120−8121.
(10) Huong, P. V.; Pommier, J. C. *Acad. Sci. Ser. C* **1977**, *285*, 519−522.
(11) Arnold, D. P. *Inorg. Chim. Acta* **1992**, *193*, 27−33.
(12) Vestling, C. S.; Downing, J. R. *J. Am. Chem. Soc.* **1939**, *61*, 3511−3513.

(13) Sturhahn, W.; Toellner, T. S.; Alp, E. E.; Zhang, X.; Ando, M.; Yoda, Y.; Kikuta, S.; Seto, M.; Kimball, C. W.; Dabrowski, B. *Phys. Rev. Lett.* **1995**, *74*, 3832−3835.
(14) Seto, M.; Yoda, Y.; Kikuta, S.; Zhang, X. W.; Ando, M. *Phys. Rev. Lett.* **1995**, *74*, 3828−3831.
(15) Chumakov, A. I.; Rüffer, R.; Grünsteudel, H.; Grünsteudel, H. F.; Grübel, G.; Metge, J.; Leupold, O.; Goodwin, H. A. *Europhys. Lett.* **1995**, *30*, 427−432.
(16) Sturhahn, W. *J. Phys.: Condens. Matter* **2004**, *16*, S497−S530.
(17) Zeng, W.; Silvernail, N. J.; Scheidt, W. R.; Sage, J. T. In *Nuclear Resonance Vibrational Spectroscopy (NRVS)*; Scott, R. A., Lukehart, C. M., Eds.; John Wiley & Sons: Chichester, U.K., 2007; pp 401−421.
(18) Giefers, H.; Tanis, E. A.; Rudin, S. P.; Greeff, C.; Ke, X.; Chen, C. F.; Nicol, M. F.; Pravica, M.; Pravica, W.; Zhao, J.; Alatas, A.; Lerche, M.; Sturhahn, W.; Alp, E. *Phys. Rev. Lett.* **2007**, *98*, 245502.
(19) Parshin, P. P.; Zemlyanov, M. G.; Panova, G. K.; Shikov, A. A.; Kumzerov, Y. A.; Naberezhnov, A. A.; Sergueev, I.; Crichton, W.; Chumakov, A. I.; Rüffer, R. *J. Exp. Theor. Phys.* **2012**, *114*, 440−450.
(20) Toellner, T. S.; Hu, M. Y.; Bortel, G.; Sturhahn, W.; Shu, D. *Nucl. Instrum. Methods Phys. Res. Sect. A* **2006**, *557*, 670−675.
(21) Lipkin, H. J. *Phys. Rev. B* **1995**, *52*, 10073−10079.
(22) Sturhahn, W. *Hyperfine Interact.* **2000**, *125*, 149−172.
(23) Frisch, M. J.; Trucks, G. W.; Schlegel, H. B.; Scuseria, G. E.; Robb, M. A.; Cheeseman, J. R.; Zakrzewski, V. G.; Montgomery, J. A., Jr.; Stratmann, R. E.; Burant, J. C.; Dapprich, S.; Millam, J. M.; Daniels, A. D.; Kudin, K. N.; Strain, M. C.; Farkas, O.; Tomasi, J.; Barone, V.; Cossi, M.; Cammi, R.; Mennucci, B.; Pomelli, C.; Adamo, C.; Clifford, S.; Ochterski, J.; Petersson, G. A.; Ayala, P. Y.; Cui, Q.; Morokuma, K.; Salvador, P.; Dannenberg, J. J.; Malick, D. K.; Rabuck, A. D.; Raghavachari, K.; Foresman, J. B.; Cioslowski, J.; Ortiz, J. V.; Baboul, A. G.; Stefanov, B. B.; Liu, G.; Liashenko, A.; Piskorz, P.; Komaromi, I.; Gomperts, R.; Martin, R. L.; Fox, D. J.; Keith, T.; Al-Laham, M. A.; Peng, C. Y.; Nanayakkara, A.; Challacombe, M.; Gill, P. M. W.; Johnson, B.; Chen, W.; Wong, M. W.; Andres, J. L.; Gonzalez, C.; Head-Gordon, M.; Replogle, E. S.; Pople, J. A. *Gaussian 98*, revision A.3; Gaussian, Inc.: Pittsburgh, PA, 1998.
(24) Mason, S. F. *J. Chem. Soc.* **1958**, 976−982.
(25) Bellamy, L. J. *The Infrared Spectra of Complex Molecules*; Wiley: New York, 1975.
(26) Li, X. Y.; Czernuszewicz, R. S.; Kincaid, J. R.; Stein, P.; Spiro, T. G. *J. Phys. Chem.* **1990**, *94*, 47−61.
(27) Ogoshi, H.; Masai, N.; Yoshida, Z.; Takemoto, J.; Nakamoto, K. *Bull. Chem. Soc. Jpn.* **1971**, *44*, 49−51.
(28) Xu, K. W.; Rankin, J. G.; Lash, T. D. *Vib. Spectrosc.* **1998**, *18*, 175−186.
(29) Ogoshi, H.; Watanabe, E.; Yoshida, Z.; Kincaid, J.; Nakamoto, K. *J. Am. Chem. Soc.* **1973**, *95*, 2845−2849.
(30) Mitchell, M. L.; Li, X.-Y.; Kincaid, J. R.; Spiro, T. G. *J. Phys. Chem.* **1987**, *91*, 4690−4696.
(31) Sage, J. T.; Paxson, C.; Wyllie, G. R. A.; Sturhahn, W.; Durbin, S. M.; Champion, P. M.; Alp, E. E.; Scheidt, W. R. *J. Phys.: Condens. Matter* **2001**, *13*, 7707−7722.
(32) Smith, M. C.; Xiao, Y.; Wang, H.; George, S. J.; Coucouvanis, D.; Koutmos, M.; Sturhahn, W.; Alp, E. E.; Zhao, J.; Cramer, S. P. *Inorg. Chem.* **2005**, *44*, 5562−5570.
(33) Xiao, Y.; Koutmos, M.; Case, D. A.; Coucouvanis, D.; Wang, H.; Cramer, S. P. *Dalton Trans.* **2006**, *18*, 2192−2201.
(34) Leu, B. M.; Ching, T. H.; Zhao, J.; Sturhahn, W.; Alp, E. E.; Sage, J. T. *J. Phys. Chem. B* **2009**, *113*, 2193−2200.
(35) Zeng, W.; Barabanschikov, A.; Wang, N.; Lu, Y.; Zhao, J.; Sturhahn, W.; Alp, E. E.; Sage, J. T. *Chem. Commun.* **2012**, *48*, 6340−6342.
(36) Leu, B. M.; Silvernail, N. J.; Zgierski, M. Z.; Wyllie, G. R. A.; Ellison, M. K.; Scheidt, W. R.; Zhao, J.; Sturhahn, W.; Alp, E. E.; Sage, J. T. *Biophys. J.* **2007**, *92*, 3764−3783.
(37) Pavlik, J. W.; Barabanschikov, A.; Oliver, A. G.; Alp, E. E.; Sturhahn, W.; Zhao, J.; Sage, J. T.; Scheidt, W. R. *Angew. Chem., Int. Ed.* **2010**, *49*, 4400−4404.
(38) Lehnert, N.; Sage, J. T.; Silvernail, N.; Scheidt, W. R.; Alp, E. E.; Sturhahn, W.; Zhao, J. *Inorg. Chem.* **2010**, *49*, 7197−7215.
(39) Sage, J. T.; Durbin, S. M.; Sturhahn, W.; Wharton, D. C.; Champion, P. M.; Hession, P.; Sutter, J.; Alp, E. E. *Phys. Rev. Lett.* **2001**, *86*, 4966−4969.
(40) Leu, B. M.; Zgierski, M. Z.; Wyllie, G. R. A.; Scheidt, W. R.; Sturhahn, W.; Alp, E. E.; Durbin, S. M.; Sage, J. T. *J. Am. Chem. Soc.* **2004**, *126*, 4211−4227.
(41) Peng, Q.; Pavlik, J. W.; Scheidt, W. R.; Wiest, O. *J. Chem. Theory Comput.* **2012**, *8*, 214−223.
(42) Lehnert, N.; Galinato, M. G. I.; Paulat, F.; Richter-Addo, G. B.; Sturhahn, W.; Xu, N.; Zhao, J. *Inorg. Chem.* **2010**, *49*, 4133−4148.
(43) Barabanschikov, A.; Demidov, A.; Kubo, M.; Champion, P. M.; Sage, J. T.; Zhao, J.; Sturhahn, W.; Alp, E. E. *J. Chem. Phys.* **2011**, *135*, 015101.
(44) Cullen, D. L.; Meyer, E. *Acta Cryst. B* **1973**, *29*, 2507−2515.
(45) Maeda, D.; Shimakoshi, H.; Abe, M.; Hisaeda, Y. *Inorg. Chem.* **2009**, *48*, 9853−9860.
(46) Li, X. Y.; Czernuszewicz, R. S.; Kincaid, J. R.; Spiro, T. G. *J. Am. Chem. Soc.* **1989**, *111*, 7012−7023.
(47) Chumakov, A. I.; Rüffer, R.; Leupold, O.; Sergueev, I. *Struct. Chem.* **2003**, *14*, 109−119.
(48) Drummond, G. S.; Kappas, A. *Proc. Natl. Acad. Sci. U.S.A.* **1981**, *78*, 6466−6470.
(49) Drummond, G. S.; Galbraith, R. A.; Sardana, M. K.; Kappas, A. *Arch. Biochem. Biophys.* **1987**, *255*, 64−74.
(50) Davari, M. D.; Bahrami, H.; Zahedi, M.; Safari, N. *Theochem−J. Mol. Struct.* **2009**, *908*, 1−11.
(51) Davari, M. D.; Bahrami, H.; Zahedi, M.; Safari, N. *Inorg. Chim. Acta* **2010**, *363*, 1577−1586.
(52) Lang, T.; Graf, E.; Kyritsakas, N.; Hosseini, M. W. *Dalton Trans.* **2011**, *40*, 3517−3523.
(53) Hu, M. Y.; Toellner, T. S.; Dauphas, N.; Alp, E. E.; Zhao, J. *Phys. Rev. B* **2013**, *87*, 064301.
(54) Arjmand, F.; Jamsheera, A. *Spectroc. Acta A* **2011**, *78*, 45−51.
(55) Komeda, S.; Casini, A. *Curr. Top. Med. Chem.* **2012**, *12*, 219−235.
(56) Portman, S.; Lüthi, H. P. *Chimia* **2000**, *54*, 766−770.